

EGFR amplification induces increased DNA damage response and renders selective sensitivity to Talazoparib (PARP inhibitor) in glioblastoma

Shaofang Wu¹, Feng Gao¹, Siyuan Zheng², Chen Zhang¹, Emmanuel Martinez-Ledesma Juan^{1,6},
Ravesanker Ezhilarasan³, Jie Ding¹, Xiaolong Li¹, Ningping Feng⁴, Asha Multani⁵, Erik P.
Sulman³, Roel Verhaak², John F. de Groot¹, Tim Heffernan⁴, W. K. Alfred Yung¹, and Dimpy
Koul^{1*}

Brain Tumor Center, Departments of ¹Neuro-Oncology and ²Genomic Medicine, ³Department of
Radiation Oncology, ⁴Applied Cancer Science Institute and ⁵Department of Genetics, The
University of Texas MD Anderson Cancer Center, Houston, Texas, USA.
⁶Tecnologico de Monterrey, Escuela de Medicina y Ciencias de la Salud, Ave. Morones Prieto
3000, Monterrey, N.L., 64710, Mexico

*Correspondence: [Dimpy Koul](mailto:dkoul@mdanderson.org), Department of Neuro-Oncology, Unit 1003, The University of
Texas MD Anderson Cancer Center, 1515 Holcombe Blvd., Houston, TX 77030. Tel: 713-834-
6202; fax: 713-834-6230; e-mail: dkoul@mdanderson.org.

Running title: EGFR as a predictor of PARP inhibitor sensitivity

Key words: PARP inhibitor, PARP/DNA complex, EGFR

Conflict of interest: W.K.A.Yung declares competing interests as an advisor in Scientific
Advisory Board for DNAtrix, Expert Advisory Board for Boehringer Ingelheim, and holding
stock of DNAtrix. Rest all authors have no conflict of Interest to disclose.

Abstract

Purpose: Exploration of novel strategies to extend the benefit of PARP inhibitors beyond BRCA-mutant cancers is of great interest in personalized medicine. Here we identified EGFR-amplification as a potential biomarker to predict sensitivity to PARP inhibition, providing selection for GBM patient population who will benefit from PARP inhibition therapy.

Experimental Design: Selective sensitivity to PARP inhibitor talazoparib was screened and validated in two sets [test set (n=14) and validation set (n=13)] of well-characterized patient-derived glioma-sphere-forming cells (GSC). FISH was used to detect EGFR copy number. DNA damage response following talazoparib treatment was evaluated by γ H2AX and 53BP1 staining and neutral comet assay. PARP-DNA trapping was analyzed by subcellular fractionation. The selective monotherapy of talazoparib was confirmed using in-vivo glioma models.

Results: EGFR-amplified GSCs showed remarkable sensitivity to talazoparib treatment. EGFR-amplification was associated with increased ROS and subsequent increased basal expression of DNA repair pathways to counter elevated oxidative stress, and thus rendered vulnerability to PARP inhibition. Following talazoparib treatment, EGFR-amplified GSCs showed enhanced DNA damage and increased PARP-DNA trapping which augmented the cytotoxicity. EGFR-amplification associated selective sensitivity was further supported by the in vivo experimental results showing that talazoparib significantly suppressed tumor growth in EGFR-amplified subcutaneous models but not in non-amplified models.

Conclusion: EGFR-amplified cells are highly sensitive to talazoparib. Our data provide insight into the potential of using EGFR amplification as a selection biomarker for the development of personalized therapy.

Translational Relevance:

EGFR-amplification occurs in approximately 50% of glioma patients. A total of 27 patient-derived GSCs were characterized and screened for PARP inhibitor talazoparib sensitivity. GSCs harboring EGFR-amplification showed significantly higher sensitivity to talazoparib treatment. EGFR-amplification was associated with elevated ROS levels, and gene enrichment analysis revealed DNA repair pathways were upregulated to counter elevated oxidative stress, and thus rendered vulnerability to PARP inhibition. Inhibition of PARP by talazoparib in EGFR-amplified cells led to unrepaired DSB and increased PARP-DNA trapping. The selective sensitivity was further supported by the in vivo results showing that talazoparib significantly suppressed tumor growth in two EGFR-amplified subcutaneous models but not in the two non-amplified models. Hence, our results demonstrated that EGFR-amplification is a novel predictive biomarker of response to PARP inhibitor talazoparib therapy in GBM.

Introduction

Glioblastoma (GBM) is one of the most aggressive and lethal human cancer. Despite advances in surgery, radiotherapy and chemotherapy, the median overall survival is less than 15 months (1-3). Mutations and copy number aberrations of EGFR have been identified as one of the most frequent genetic events in GBM by The Cancer Genome Atlas (TCGA) (4,5). EGFR amplification/mutation was associated with significant elevations in total EGFR expression and phosphorylation and activation of multiple oncogenic pathways.

Glioma-sphere-forming cells (GSC) are derived from primary GBM and cultured in minimal medium containing growth factors to select the cells with sphere-forming capacity. These sphere forming cells are often termed ‘glioma stem-like cells’ as they have the capacity for self-renewal and multipotency (6,7), and the capacity to form gliomas which reflect the histopathological heterogeneity of the parental tumors. These cells are thought to be responsible for tumor progression, recurrence and resistance to radiation and conventional chemotherapy (8,9), and thus represent a vital target for cancer therapy. A growing body of evidence demonstrated, although still controversial, that GSCs had higher activation of DNA damage response (DDR) and single-strand break response (SSBR) at both the basal level and after ionizing radiation to tolerate DNA damage stress and oxidative stress (8,10-12). The reliance on DNA damage repair to handle additional genotoxic stress in GSCs suggested that targeting key DNA damage repair pathway molecules would be an effective therapy for GBM.

Poly-ADP-ribose polymerase 1 (PARP1) is an enzyme that catalyzes the transfer of ADP-ribose polymers to substrates, including numerous DNA repair enzymes to sense DNA lesions, activates DNA damage responses, and facilitates DNA damage repairs. The central role of PARP in DNA damage response, particularly in SSBR, makes it a promising therapeutic

target. Multiple PARP inhibitors have been developed in pre-clinical and clinical studies in various tumors including GBM (13). Combination of PARP inhibitors olaparib and veliparib with TMZ has been studied in a phase 1 trial and a phase 2/3 trials, respectively. However, excessive toxicity in combination with TMZ limited its efficacy and led to clinical trial failure (14,15). Talazoparib, a novel oral PARP inhibitor with greater in vitro activity than any other PARP inhibitor currently in development (16,17), showed promising single-agent lethality in advanced ovarian and breast cancer harboring deleterious BRCA1/2 mutations. However, BRCA mutations are rare in other cancers including GBM (18,19), which limited the application of talazoparib therapy. Talazoparib is currently in clinical trials for GBM (NCT02116777). Exploration of novel strategies and identifying predictive biomarkers to select GBM patients who are most likely to benefit from talazoparib treatment is urgently needed.

In the current study, using two sets of GSCs, we demonstrated that talazoparib monotherapy selectively inhibited the proliferation of EGFR-amplified GSCs in vitro and suppressed EGFR-amplified tumor progression in GSC xenograft models. Our data suggested that EGFR-amplification may be a biomarker to predict sensitivity to talazoparib treatment in GBM, providing selection of patient populations who will benefit from talazoparib treatment.

Materials and Methods

Cell lines and reagents

The GSC lines were established by isolating neurosphere-forming cells from fresh surgical specimens of human GBM tissue from 2005 through 2008, as described previously (20). The study was approved by the Institutional Review Board of MD Anderson Cancer Center, and informed consent was obtained from all subjects. GSC lines were cultured in DMEM/F12 medium containing B27 supplement (Invitrogen, Grand Island, NY), basic fibroblast growth factor, and epidermal growth factor (20 ng/ml each). All GSCs used in the study were less than 15 passages. Cells were authenticated by testing short tandem repeats using the Applied Biosystems AmpFISTR Identifier kit (Foster City, CA). The last authentication test was performed in July 2017. All cell lines were tested negative for mycoplasma contamination by using MycoAlert Detection Kit (Lonza, Alpharetta, GA). Talazoparib was from WuXi AppTec (Wuxi, Jiangsu, China). Olaparib, veliparib and pamiparib were from Selleckchem (Houston, TX). MnTBAP was from Abcam (Cambridge, MA, USA). For in vitro use, all inhibitors were dissolved in dimethyl sulfoxide (Sigma-Aldrich, St. Louis, MO).

Cell proliferation assay

Cells were treated with talazoparib in triplicate for 5 days, and cell proliferation was determined using the CellTiter-Blue viability assay (Promega, Madison, WI). The IC₅₀ value was calculated as the mean drug concentration required to inhibit cell proliferation by 50% compared with vehicle-treated controls using GraphPad software (GraphPad Software, Inc., La Jolla, CA).

Subcellular fractionation assay

To detect chromatin-bound PARP, cells were collected and cytoplasmic, nuclear soluble, and chromatin-bound proteins were fractionated using a subcellular protein fractionation kit from

Thermo Scientific (#78840), following the manufacturer's instructions (17). Immunoblotting was carried out using standard procedures. Actin was blotted for cytoplasmic fraction marker, Lamin B for nuclear soluble marker, and Histone H3 for chromatin-bound marker.

Fluorescence in situ hybridization (FISH)

Exponentially growing cells were treated with colcemid (0.04 µg/mL) for 2 h and chromosomes were prepared by conventional fixation. FISH assay was performed on the slides using EGFR FISH probe from Empire Genomics (Buffalo, NY) following the manufacturer's instructions with slight modifications. Briefly, the probe was applied on the slide and covered with a glass coverslip and sealed with rubber cement. The slides were then denatured at 70 °C using ThermoBrite system (Abbott Laboratories, IL) and incubated at 37 °C overnight. The slides were then washed using 2XSSC at 45 °C for 1-2 mins, rinsed in 0.05% Tween 20 in PBS counterstained with DAPI, and analyzed under Nikon ECLIPSE 80i fluorescent microscope. A minimum of 50 cells were examined to score the number of fluorescent signals.

Immunofluorescence staining

Cells were seeded onto Lab-Tek II tissue culture slides (Thermo Fisher) and treated with talazoparib and washed-out for indicated time. Cells were fixed with 4% paraformaldehyde, permeabilized with 0.2% Triton X-100, and blocked with 5% BSA in PBS and then stained overnight at 4°C with anti-53BP1 antibody (Santa Cruz) and anti-gamma H2AX (phospho S139) antibody (Abcam). Cells were washed with PBS, stained with secondary antibodies (Alexa Fluor 594 donkey anti-rabbit IgG; Alexa Fluor 488 donkey anti-goat IgG; Invitrogen) for 1 hour. The cells were counterstained with Vecta shield sealant containing 4',6-diamidino-2-phenylindole (DAPI) (Vector laboratories, California, USA). The percentage of cells displaying foci was quantified by counting 5 random fields.

Measurement of ROS activity

To measure ROS activity, GSCs were stained with a CM-H₂DCFDA probe, according to the manufacturer's instructions (Molecular Probes, Invitrogen, Carlsbad, CA). In brief, cells were dissociated with accutase to single cells, suspended in pre-warmed HBSS containing a 10 μ M CM-H₂DCFDA probe, and incubated at 37°C for 30 min. Cells were then acquired with FACS (BD Biosciences, San Jose, CA) and analyzed using FlowJo software (Tree Star, Inc., Ashland, OR).

Neutral comet assay

Neutral comet assays were performed using an OxiSelect Comet Assay Kit (Cell Biolabs, USA) per manufacture's protocol. Briefly, cells were dissociated with Accutase and washed with PBS, and replicates were suspended in OxiSelect comet agarose (Cell Biolabs, USA). Neutral electrophoresis was conducted at 30 V for 30 min. Data was collected with a fluorescent microscope with a FITC filter and analyzed using the OpenComet software (21). All steps after agarose treatment were conducted in the dark to prevent additional DNA damage.

Animal studies

All animal studies were approved by the institutional review board of The University of Texas MD Anderson Cancer Center (Houston, Texas). Cells were transfected with MSCV-Luciferase-EF1 α -copGFP-T2A-Puro BLIV 2.0 Lentivector (SBI System Biosciences, Palo Alto, CA) to generate luciferase expressing cells for in vivo imaging. To create subcutaneous tumor model, luciferase expressing cells (5×10^6 cells) were implanted into the hind flanks of 4-6 weeks old male nu/nu mice. For intracranial models, luciferase expressing cells (0.5×10^6) were implanted intracranially into nude mice using a previously described guide-screw system (22). Starting on day 14 after tumor cell implantation, mice were treated with 0.33 mg/kg talazoparib by oral

gavage. The treatment frequency was twice a day for 5 days, with 2 days off between treatments, for a total duration of 6 weeks. Tumor growth and development was visualized and quantified using the IVIS Spectrum in vivo imaging system. Mice were monitored daily and euthanized when they became moribund. The whole brains from the intracranial models and the tumors from subcutaneous models were collected and preserved in formaldehyde solution for future use.

Computational analysis

Mutations and copy number alterations of GSCs were determined by exome sequencing (Illumina HiSeq) and Affymetrix OncoScan FFPE V2 arrays. In this study, we focused on the prominent driver genes p53, EGFR, and PTEN that also showed frequent mutations and copy number alterations in GBM. Gene set enrichment analysis (GSEA) was performed with a pre-ranked list of genes. To rank genes, EGFR-amplified was compared with non-amplified GSCs to obtain differentially expressed genes using limma (23). Then, genes were ranked according to p-value and Fold-Change (FC) multiplying $-\log_{10}(\text{p-value})$ by the FC sign. We ran GSEA using the gene sets from the Canonical Pathways compendia (C2) version 6.1 from MsigDB (24).

Statistical analysis

The statistical comparison was performed using Student's t-test or Fisher's exact test, as appropriate. The results are presented as the mean of at least 3 independent experiments. All tests were 2-sided. Statistical analyses were carried out using GraphPad Prism software. A P-value of <0.05 was considered statistically significant. Survival curves were plotted using the Kaplan-Meier method, and log-rank tests were used to compare survival curves between groups.

Results

PARP inhibition by talazoparib selectively suppresses the proliferation of EGFR-amplified GSCs

To test the anti-proliferative activity of talazoparib, we first used a test set of 14 GSCs to study a dose-response profile to talazoparib (Fig. 1A). The dose of talazoparib required to inhibit 50% of cell growth (IC_{50}) varied widely from 4.3 nM to over 1500 nM (Fig. 1B). Of 14 GSCs, 7 were sensitive to talazoparib, with IC_{50} less than 300 nM, and the other 7 were relatively resistant, with IC_{50} higher than 300 nM.

To identify potential markers of talazoparib sensitivity, we studied genetic status of most frequently mutated genes in GBM. The mutation, amplification/deletion of p53, EGFR, PTEN, PDGFRA and MET were determined by whole genome sequencing as well as OncoScan array. As shown in Fig. 1B, EGFR amplification was one of the main determinants in 6 of 7 sensitive GSCs (85.7%); 0 out of 7 resistant GSCs (0%) showed amplification of EGFR ($p=0.005$, Fisher exact test). We then used a validation set of 13 GSCs to determine the dose-response to talazoparib (Fig. 1C). Six GSCs showed an IC_{50} less than 300 nM. Similar to the test set, 5 of the 6 sensitive GSCs in the validation set were EGFR amplified (83.3%) (Fig. 1D); 1 out of 7 resistant GSCs (14.3%) was EGFR amplified ($p=0.029$, Fisher exact test). Collectively, the results from 27 cell GSC lines revealed that EGFR-amplified cells have significantly lower IC_{50} than do EGFR non-amplified cells ($p<0.05$, Fig. 1E). In contrast, the sensitivity was not associated with alteration of PTEN, p53 or CDKN2A, the other three most frequent genetic alterations in GBM (Fig. 1F - H).

EGFR amplification was evaluated by copy number variation (CNV) as determined by OncoScan array and stratified according to a threshold of $CNV \geq 2$ (Fig. 1I). EGFR

amplification was further validated by fluorescence in situ hybridization (FISH) (Fig. 1J). At least 50 cells for each line were randomly examined for EGFR FISH signals. Consistent with CNV results, EGFR amplified cells displayed higher FISH signals (average signals ranges from 20 to ≥ 30 spots per cell), with majority of the cells displaying ≥ 10 signals (Fig. 1K). Furthermore, we performed western blot to detect EGFR protein expression and the canonical downstream signaling. EGFR protein expression is indeed higher in EGFR amplified group compared to non-amplified group. pStat3-Y705, and pAKT-T308 to a less extent, was elevated in amplified group, confirming that EGFR signaling is activated in amplified group (Fig. 1L and Supplemental Fig. S1).

Talazoparib selectively depleted the subpopulation with high EGFR copy number

EGFR amplification in GBM tumors is heterogeneous (25-27). This heterogeneity is also noted in our GSCs. For example in GSC262, 76% of cells displayed very high EGFR signal (>35 signals/cell) and 24% of cells have a low EGFR signal less than 10. For GSC11, 68% of cells displayed very high EGFR signal and 32% of cells have a low EGFR signal less than 10 (Supplemental Fig.2A). Therefore, we ask if talazoparib preferentially kills the subpopulation of cells with high EGFR copy number and if so, will talazoparib treated cells lose EGFR amplification. To answer this question, we treated GSC262 and GSC11 cells with talazoparib and the post treatment living cells were sorted by FACS and the EGFR copy number were evaluated by FISH. As expected, only low EGFR copy number cells (< 10 signals/cell) survived after talazoparib treatment (Supplemental Fig. 2A-C) and the cells with greater than 35 signals were completely lost (Supplemental Fig. 2C). Further we showed that total EGFR protein level was also decreased after talazoparib treatment for 6 days (Supplemental Fig. 2D), confirming that talazoparib selectively depleted the subpopulation of cells with high EGFR copy number.

Depletion of EGFR renders resistance to talazoparib

To further examine the role of EGFR in talazoparib sensitivity, we knock out EGFR in an EGFR-amplified GSC line GSC262 using the CRISPR gene editing method (28,29) (Fig. 2A). Two clones were isolated and sequenced to confirm that EGFR gene was edited. Knock-out of EGFR slowed down cell proliferation by 20% (data not shown). As shown in Fig. 2A, expression of EGFR and subsequent p-EGFR-Y1068 were completely depleted, and pSTAT3-Y705 was markedly decreased, confirming EGFR expression and signaling was inhibited by EGFR knock-out. Further, we showed that knock-out of EGFR renders cells resistant to talazoparib, as shown by the increased IC_{50} (Fig. 2B and C). We also knocked down EGFR in amplified GSC274 and GSC11 using two shRNAs targeting EGFR. Although shRNA being less effective to deplete EGFR expression in comparison to CRISPR/Cas9/sgRNA, it is noteworthy to observe a moderate resistance to talazoparib (Fig. 2D-I), further confirming EGFR mediated sensitivity to talazoparib. In contrast, we over expressed wild type EGFR (EGFR-wt) and kinase-inactive EGFR (EGFR-KI) in a non-amplified/ resistant cell line GSC272. pEGFR-Y1068 and pSTAT3-Y705 was increased in EGFR-wt cells but not in EGFR-KI cells, confirming that EGFR signaling was activated by EGFR-wt overexpression but not EGFR-KI overexpression (Fig. 2J). Overexpression of EGFR-wt sensitized cells to talazoparib (Fig. 2K and L). However, overexpression of EGFR-KI failed to sensitize cells to talazoparib (Fig. 2K and L), suggesting that kinase activity is required for EGFR-mediated inhibition of cell proliferation by talazoparib.

Talazoparib sensitivity was correlated with increased ROS production in EGFR-amplified GSCs

Elevated ROS levels has been reported to be associated with EGFR activity leading to sensitivity to PARP inhibition (30). To determine if EGFR amplification induce ROS in GSCs and resultant sensitivity to talazoparib, we tested ROS levels in 10 GSCs. EGFR-amplified GSCs (n=5) contain higher basal ROS levels than non-amplified GSCs (n=5) (p=0.026) (Fig. 3A). EGFR amplification appears to be important for ROS production and sensitivity to talazoparib as knock-out of EGFR in amplified cells reduced ROS levels (Fig. 3B) (p=0.024) and decreased sensitivity to talazoparib (Fig. 2C) (p<0.0001).

To determine whether ROS contributes to EGFR-mediated talazoparib sensitivity, we treated EGFR-amplified cells with ROS-specific inhibitor MnTBAP. Our data showed that MnTBAP treatment desensitized GSCs to talazoparib (Fig. 3C). In contrast, MnTBAP failed to desensitize EGFR non-amplified GSCs (Fig. 3C). More importantly, while MnTBAP significantly desensitized GSC262 vector cells, it has very slight effect on CRISPR EGFR knock-out cells regarding talazoparib response (Fig. 3D), indicating that EGFR-amplification mediated ROS accumulation and sensitivity to talazoparib.

To evaluate if the excess ROS induces oxidative DNA damage, we evaluated the level of 8-hydroxy-2'-deoxyguanosine (8-OHdG), the most representative product of oxidative modifications of DNA and predominant form of free radical-induced oxidative lesions in a panel of EGFR-amplified and non-amplified GSCs. Interestingly, the basal level of 8-OHdG pre-talazoparib treatment showed no difference between two groups (Fig. 3E). However talazoparib treatment induced 8-OHdG in EGFR-amplified cells but not in non-amplified cells (Fig. 3E). These observations suggested that the ROS-induced oxidative lesions were countered by enhanced DNA damage repair, conferring a likely reliance on the key SSBR mediator PARP in EGFR-amplified GSCs.

EGFR-amplified cells have increased DNA damage repair capacity

Next, we evaluated whether the increased oxidative stress induced DNA damage response components in EGFR-amplified GSCs. To gain better understanding of the relationship between EGFR and DNA damage repair, we analyzed the RNA-sequencing data of 27 GSC lines (12 EGFR-amplified and 15 non-amplified). A gene set enrichment analysis revealed several DNA damage response and DNA repair pathways were significantly and positively correlated with EGFR amplification, including G2/M checkpoints (NES=1.97, $p=0.000$, rank=2), homologous recombination (NES=1.86, $p=0.0034$, rank=11), double strand break repair (NES=1.80, $p=0.0036$, rank=14), global genome nucleotide excision repair (GG-NER) (NES=1.56, $p=0.026$, rank=36), activation of ATR in response to replication stress (NES=1.97, $p=0.000$, rank=6) (Fig. 4A). This data was further substantiated by analysis of gene expression profiling data from the TCGA GBM database that showed GG-NER genes were also enriched in EGFR-amplified patient tissue samples (Supplemental Fig. S3), thus suggesting the clinical relevance of this correlation in clinical settings. These results support the hypothesis that the EGFR amplified group has more active DNA repair machinery through coordinated overexpression of several key genes in the pathway.

Next we tested if blocking DNA repair with a PARP inhibitor would result in DSB accumulation in EGFR-amplified cells. We used immunofluorescence to detect γ H2AX foci and 53BP1 foci as indicator of DNA breaks. We showed that talazoparib treatment induced γ H2AX foci and 53BP1 foci in EGFR-amplified GSC262 and GSC274 cells but not in the non-amplified GSC23 and GSC20 cells (Fig. 4B). Talazoparib-induced DSBs in EGFR-amplified cells is further confirmed by comet assay. As shown in Fig. 4C, comet tail moments were induced by talazoparib in GSC262 vector cells as early as 24-hour time point and persists even at 72-hour

time point whereas less induction was observed in EGFR knock out cells even at 72 hour time lapse. The DNA in tail are represented as percentage of moments at 0-72 hours span increasing from 5% to 80% in GSC262 amplified cells and percentage of DNA moment is decreased in EGFR knock-out cells in comparison to parent cells.

To further prove that the EGFR-amplified cells have increased repair capacity to counter DNA damage, we challenged the cells with talazoparib for 72hours to block DNA repair and allowed DNA damage to accumulate, after which talazoparib medium was replaced with fresh medium to allow cells to recover from damage for 24 hrs, 48 hrs and 72 hrs, and DNA damage was assessed by γ -H2AX and 53BP1 foci formation. As show in Fig. 4D, in GSC262 (EGFR-amplified cells), talazoparib treatment resulted in accumulation of DNA damage as indicated by the co-localization of γ -H2AX and 53BP1 foci. After talazoparib washout, both the foci number and the percentage of positive cells decreased in a time-dependent manner, indicating the high repair capacity of the EGFR-amplified cells once the repair inhibition was removed. In EGFR knock-out cells, block of repair by talazoparib treatment resulted in a weak DNA damage as indicated by the less percentage of positive cells with less foci number. After talazoparib washout, the cells recovered in a much slower way.

Similarly, in the EGFR-non-amplified GSC272 cells, blocking of DNA repair by talazoparib treatment resulted in a weak DNA damage as indicated by the low percentage of positive cells with few foci number (Fig. 4E). After talazoparib washout, the cells recovered slowly. In contrast, in GSC272 EGFR overexpressed cells, talazoparib treatment resulted in a strong DNA damage as indicated by the increased foci number and the percentage of positive cells. After talazoparib washout, the foci number and the percentage of positive cells decreased rapidly, indicating the DNA damage was repaired efficiently.

These findings prompted us to conclude that EGFR-amplified GSCs have increased DNA damage repair capacity and are reliant on PARP to tolerate oxidative base damage and maintain genomic stability. This is further supported by the observation that PARP inhibition by talazoparib resulted in remarkable apoptosis in EGFR-amplified GSCs (Supplemental Fig. S4) due to increased DNA damage and inhibition of DNA repair.

Talazoparib is efficient at trapping PARP-DNA complex in EGFR-amplified GSCs

We next investigated the mechanism of response to talazoparib in EGFR-amplified and non-amplified GSCs. We first tested the potency of talazoparib in inhibiting total cellular poly (ADP-ribosyl)ation (PARylation) by Western blot against PAR. As shown in Supplemental Fig. S5, talazoparib reduced total PARylation levels at 10 nM concentrations in both sensitive (GSC262, EGFR-amplified, IC_{50} =133 nM) and resistant cells (GSC272, EGFR-non-amplified, IC_{50} =6930 nM). Although the IC_{50} of talazoparib varies between the two groups, the concentration needed to fully inhibit PARylation was similar and was much lower than the IC_{50} , indicating that the differential response to talazoparib is not purely mediated by the enzymatic inhibition of PARP.

In addition to inhibiting the enzymatic activity of PARP, trapping PARP on damaged DNA has been identified as an important and major mechanism that accounts for the cytotoxicity of PARP inhibitors (31). Since EGFR-amplified cells have more ROS-induced DNA damage accumulated than non-amplified cells following PARP inhibition, and as PARP selectively binds to damaged DNA, we determined whether talazoparib trapped more PARP-DNA complex in EGFR-amplified GSCs than in non-amplified cells as a mechanism to account for enhanced activity in amplified cells. An analysis of the subcellular fraction revealed that talazoparib treatment trapped significant chromatin-bound PARP in GSC262 (Fig. 5A) and GSC274 (Fig. 5B) cells, which are both talazoparib sensitive and EGFR-amplified. About 42.1% of total

nuclear PARP was trapped at DNA at day 5 in GSC262 (Fig. 5A), and about 54.6% of total nuclear PARP was trapped at DNA at day 5 in GSC274 (Fig. 5B). However, chromatin-bound PARP was not induced by talazoparib in resistant and non-amplified GSC272 cells (Fig. 5C). We further showed that knock-out of EGFR in GSC262 cells blocked talazoparib-induced PARP-DNA complex formation (Fig. 5D), while overexpression of EGFR in GSC272 enhanced talazoparib-induced PARP-DNA complex formation (Fig. 5E). Collectively, these results suggested that talazoparib was able to trap more PARP-DNA complexes in EGFR-amplified GSCs, eventually inducing cell death in these GSCs.

EGFR-amplified GSCs showed selective sensitivity to pamiparib but not to olaparib or veliparib

To test if the EGFR-associated sensitivity can be observed with other PARP inhibitors and if PARP-DNA trapping capability of PARP inhibitors is important for cellular toxicity, we determined the efficacy of three other clinical PARP inhibitors, pamiparib, veliparib and olaparib in 14 GSCs. Pamiparib showed selective sensitivity in EGFR-amplified GSCs (Supplemental Fig. S6A-C). In contrast, olaparib and veliparib did not show any selective response in EGFR-amplified GSCs (Supplemental Fig. S6D-I). Consistent with previous reports (17,31), our study also observed that pamiparib and talazoparib have stronger PARP-DNA trapping capacity than olaparib and veliparib (Supplemental Fig. S6J), suggesting a role of PARP-trapping on damaged DNA in toxic effects induced by talazoparib and pamiparib.

Talazoparib selectively inhibits EGFR-amplified tumors in xenograft models

The toxicity of talazoparib was evaluated in nude mice after administering a daily dose of 0.33mg/kg (BID, Mon-Fri) for 6 weeks. Body weight was monitored every two weeks, and facial vein sampling was performed at day 42 to collect blood samples for hematology analysis.

Talazoparib was well tolerated with no significant decrease in body weight (Supplemental Fig. S7A), white blood cell count (Supplemental Fig. S7B), red blood cell count (Supplemental Fig. S7C) or hemoglobin (Supplemental Fig. S7D).

To determine whether there is an EGFR-amplification-dependent response to talazoparib *in vivo*, we established two EGFR-amplified models (GSC262 and GSC11) and two non-amplified models (GSC272 and GSC23). We observed talazoparib treatment induced a significant reduction in tumor size in GSC262 model (fold change=12.4 at day 43; $p=0.0018$) (Fig. 6A) and in GSC11 model (Fold change=5.2 at day 34; $P=0.0018$) (Fig. 6B). In contrast, talazoparib did not suppress tumor growth for GSC23 and GSC272 (Fig. 6C and D), further confirming *in vivo* antitumor activity of talazoparib in EGFR-amplified tumors.

We evaluated the DNA damage and apoptosis in xenograft tumor tissues by analyzing expression of DNA double strand break marker γ H2AX and apoptosis marker cleaved Caspase-3. Consistent with *in vitro* data, talazoparib treatment resulted in significant γ H2AX and cleaved Caspase-3 positive cells in the EGFR-amplified GSC262 and GSC11 xenograft tumors, but not in the non-amplified GSC272 or GSC23 xenograft tumors (Fig. 6E). In line with this observation, talazoparib treatment resulted in an increase of TUNEL-positive cells in EGFR-amplified GSC262 and GSC11 but not in the non-amplified GSC23 or GSC272 (Fig. 6F). Taken together, our data suggest EGFR-amplified tumor cells exhibited enhanced DNA damage and apoptosis after talazoparib treatment.

In vivo therapeutic efficacy of talazoparib in intracranial models

The *in vivo* efficacy of talazoparib was further tested in orthotopic intracranial xenografts. Nude mice with intracranial implantation of GSC262 cells (EGFR-amplified) and GSC272 cells

(EGFR-non-amplified) were treated with vehicle or talazoparib at 0.33 mg/kg BID for 6 weeks. In GSC262 model, talazoparib moderately inhibited tumor growth at day 36 ($p=0.044$) and day 42 ($p=0.04$) compared to vehicle-treated mice (Fig. 6G and H). The median survival of talazoparib-treated mice was 62 days compared to 51.5 days for vehicle-treated mice ($p=0.0039$, log-rank test) (Fig. 6I), indicating that treatment was able to delay the survival time by 20.4%. In contrast, talazoparib did not suppress tumor growth (Fig. 6J and K) nor extended animal survival in EGFR-non-amplified GSC272 intracranial model (Fig. 6L, 49.5d for control vs 47 d for talazoparib treatment).

The efficacy is relatively moderate in intracranial model compared subcutaneous model, therefore we tested if the moderate intracranial efficacy is due to limited blood-brain penetration of talazoparib. After a single PO dose (0.33 mg/kg or 0.5 mg/kg) of talazoparib, brain tissues and blood samples were harvested at different time intervals, and talazoparib levels were measured. Peak concentrations in brain and whole blood were achieved 2 hours after dosing (Supplemental Fig. S6A and B) and decreased very quickly at hour 4. The peak concentration is as high as ~400 nM in blood (Supplemental Fig. S6A), but ~15nM in brain tissue (Supplemental Fig. S6B), which is much lower than optimal concentrations associated with cell proliferation inhibition in vitro, suggesting that the moderate efficacy of the intracranial model is in fact due to the limited blood-brain penetration of talazoparib.

Discussion

We demonstrated EGFR-dependent sensitivity to the PARP inhibitor talazoparib in a large set of clinically relevant GSC lines. The EGFR-dependent talazoparib sensitivities were profound, as indicated by 30 fold difference in the median IC_{50} values of talazoparib in the EGFR-amplified

and non-amplified groups. Knock-out of EGFR using CRISPR desensitized EGFR-amplified cells to talazoparib, and overexpression of EGFR sensitized cells to PARP inhibitor, further showing that EGFR amplification is a predictor of response to talazoparib. Given that approximately 50% of GBM patients are detected with EGFR amplification (32,33), it is likely that a large subset of patients may benefit from talazoparib. EGFRV8 mutations occurred in 30% of EGFR amplified GBM (32,33). It is notable that the EGFRV8 mutation rate in GSC samples is somehow lower than that detected in GBM patients, with only two cell lines (GSC280 and GSC248) out of 27 GSC lines that showed EGFRV8 mutation. Nonetheless, GSC280 and GSC248 are among the most sensitive lines to talazoparib despite their EGFR gene copy number and EGFR expression is moderate, suggesting EGFR activation is important for talazoparib sensitivity, which is further confirmed by the result that overexpression of kinase-inactive EGFR failed to sensitize cell to talazoparib.

PTEN mutation was reported to be associated with PARP inhibitors KU0058948 and KU0059436 sensitivity in colorectal tumor cell and prostate tumor cells (34). However, in current study, we find no significant association between PTEN mutation and talazoparib sensitivity in GSC cell lines. A possible explanation for this discrepancy is that PTEN mutation are different in different tumor types, further studies comparing PTEN mutation among the different tumor types are warranted. In addition, the characteristic difference of PARP inhibitors including PARP-DNA trapping capacity and target specificity may also cause discrepancy. KU0058948 is the strongest inhibitor of PARP-3 activity (35), while talazoparib is more specific for PARP-1 and PARP-2.

In addition, IDH1 mutation and MYC amplification were also reported to confer sensitivity to PARP inhibitor in brain tumors (36-40). IDH1 mutation is a major event in low-grade gliomas (LGGs) but is quite rare in GBM. IDH1 mutation occurs in 77% LGG samples but

in only 4% GBM samples based on TCGA database, and we did not find any IDH1 mutation in 27 cell lines used in the current study. MYC amplification occurs in 0.2% primary GBM according to TCGA database. We observed 4 out of 27 cell lines have MYC amplification, and notably 3 cell lines are sensitive and 1 cell line is resistant to talazoparib, suggesting a possible association but due to limited cell lines, statistical significance was not observed for MYC amplification.

Numerous studies have suggested that EGFR activation induces multiple cellular stresses, including increased oxidative stress, proliferation stress and replication stress, all leading to DNA damage (30), requiring increased DNA repair capacity to maintain genomic stability, and thus providing vulnerability to DNA repair targeted therapy. Here, we showed that ROS level is higher in the EGFR amplified cells compared with that in the EGFR-non-amplified cells. Knock-out of EGFR by CRISPR decreased ROS level, further confirmed that EGFR amplification leads to ROS production. ROS inhibitor MnTBAP, which suppressed ROS production, desensitized EGFR-amplified cells, suggesting that the increased ROS level is associated with talazoparib sensitivity. Our finding is consistent with previous report showing correlation between increased EGFR activity, ROS, and PARP inhibitor sensitivity by testing six primary GBM cell lines with varying EGFR expression (30). However, due to the limited number of cell lines used in this study, a robust association between EGFR expression and PARP inhibition sensitivity cannot be reached. In the current study, we used a total of 27 cell lines to show that EGFR amplification renders selective sensitivity to PARP inhibitor. Our study indicated EGFR amplification could serve as a genetic marker, which is an easier selection marker than the detection of EGFR activity and ROS level, for PARP inhibitor-responsive patients.

Although accumulating evidence support that EGFR activation results in elevated ROS,

the underlying mechanisms vary and remain to be further explored. EGFR has been reported to activate NADPH oxidase to generate excessive ROS production by activating multiple possible molecules/pathways (41-43). Furthermore, ROS not only functions as a mediator of the EGFR signaling pathway, but also as a regulator of EGFR protein activity. EGFR-mediated signaling resulted in H₂O₂ production and oxidation of downstream proteins (44), meanwhile, H₂O₂-induced sulfenylation of cysteine (Cys797) can enhance EGFR tyrosine kinase activity (45), and high ROS levels can trigger overoxidation of the Met residue of EGFR^{T790M} and shut down the EGFR downstream survival pathway (46). The crosstalk between ROS and EGFR suggested that modulating ROS levels is a feasible strategy to overcome drug resistance. In this study, we have clearly shown that EGFR amplification induced excessive ROS production, and ROS scavenger MnTBAP desensitized cells to talazoparib treatment.

Gene set enrichment analysis showed EGFR-amplified GSCs as well as TCGA GBM tumors have a more active DNA repair machinery as a result of the coordinated upregulation of several DNA repair pathways. We further assessed the DNA repair capacity of EGFR-amplified and non-amplified cells by washout experiments. DNA damage accumulated in EGFR amplified or overexpressed cells after talazoparib treatment and decreased rapidly following removing DNA damage repair inhibition by washing out of talazoparib, further demonstrating the increased DNA repair capacity of EGFR amplified cells in response to the increased DNA damage in these cells.

We found that more PARP-DNA complexes were trapped by talazoparib in EGFR-amplified cells than in non-amplified cells, confirming that more DNA breaks resulted from excessive ROS induced by EGFR amplification. Overall, our results suggest that EGFR-associated and drug-specific sensitivities are associated with the PARP-DNA trapping in EGFR amplified cells.

EGFR-associated sensitivity was further evaluated in our *in vivo* studies. The significant inhibition of tumor growth in the two EGFR-amplified but not in the two non-amplified subcutaneous models confirmed the EGFR-amplification-dependent selective response to talazoparib *in vivo*.

Collectively, we reported that EGFR amplification leads to elevated ROS levels, which resulted in oxidative DNA damage. To tolerate the constitutive DNA damage caused by ROS, EGFR amplified GSCs exhibited enhanced DNA repair activity. Talazoparib acts in two steps. First, it inhibits PARP enzymatic activity which results in accumulated unrepaired DNA breaks in EGFR amplified GSCs. The accumulated unrepaired DNA then recruits more PARP as PARP selectively binds to damaged DNA, and DNA-PARP complex is trapped and accumulated in EGFR amplified cells, resulting in augmented cytotoxicity.

The efficacy of talazoparib in intracranial model is moderate, probably due to the limited blood-brain barrier penetration of talazoparib, a common issue for application of PARP inhibitors in GBM thus limiting its therapeutic implications (47-49). Improving brain delivery by either modifying the compound or using nanoparticle delivery system would maximize the therapeutic efficacy in GBM patients and offers an immediate opportunity for clinical translation.

Author contributions:

D Koul, W. K Alfred Yung and S Wu designed the study. S Wu, F Gao, C Zhang, J Ding, X Li and R Ezhilarasan conducted the experiment and collected the data. S Wu did the statistical analysis and prepared the manuscript. N Feng did the liquid chromatography-tandem mass spectrometry assay. S Zheng and E Juan did the bioinformatics study and interpretation. D Koul and W. K Alfred Yung revised the manuscript. A Multani did FISH assay. All authors read and approved the final manuscript.

Grant Support: This study was funded by a National Brain Tumor Society (Defeat GBM) Grant, National Foundation for Cancer Research (NFCR) to W. K. A. Yung, a SPORE grant (P50 CA127001 to F. F. Lang), and a Cancer Center Support Grant (CA016672).

Acknowledgements: The authors would like to thank Verlene Henry and Caroline Carrillo for performing animal studies and Ann Sutton in Scientific Publications department for manuscript editing.

References

1. Johnson DR, O'Neill BP. Glioblastoma survival in the United States before and during the temozolomide era. *Journal of neuro-oncology* **2012**;107(2):359-64 doi 10.1007/s11060-011-0749-4.
2. Davis FG, Freels S, Grutsch J, Barlas S, Brem S. Survival rates in patients with primary malignant brain tumors stratified by patient age and tumor histological type: an analysis based on Surveillance, Epidemiology, and End Results (SEER) data, 1973-1991. *Journal of neurosurgery* **1998**;88(1):1-10 doi 10.3171/jns.1998.88.1.0001.
3. Carro MS, Lim WK, Alvarez MJ, Bollo RJ, Zhao X, Snyder EY, *et al.* The transcriptional network for mesenchymal transformation of brain tumours. *Nature* **2010**;463(7279):318-25 doi nature08712 [pii] 10.1038/nature08712.
4. Brennan CW, Verhaak RG, McKenna A, Campos B, Noushmehr H, Salama SR, *et al.* The somatic genomic landscape of glioblastoma. *Cell* **2013**;155(2):462-77 doi 10.1016/j.cell.2013.09.034.
5. Cancer Genome Atlas Research N. Comprehensive genomic characterization defines human glioblastoma genes and core pathways. *Nature* **2008**;455(7216):1061-8 doi 10.1038/nature07385.
6. Kondo T, Setoguchi T, Taga T. Persistence of a small subpopulation of cancer stem-like cells in the C6 glioma cell line. *Proc Natl Acad Sci U S A* **2004**;101(3):781-6 doi 10.1073/pnas.0307618100.
7. Singh SK, Hawkins C, Clarke ID, Squire JA, Bayani J, Hide T, *et al.* Identification of human brain tumour initiating cells. *Nature* **2004**;432(7015):396-401 doi 10.1038/nature03128.
8. Bao S, Wu Q, McLendon RE, Hao Y, Shi Q, Hjelmeland AB, *et al.* Glioma stem cells promote radioresistance by preferential activation of the DNA damage response. *Nature* **2006**;444(7120):756-60 doi 10.1038/nature05236.
9. Liu G, Yuan X, Zeng Z, Tunici P, Ng H, Abdulkadir IR, *et al.* Analysis of gene expression and chemoresistance of CD133+ cancer stem cells in glioblastoma. *Mol Cancer* **2006**;5:67 doi 10.1186/1476-4598-5-67.
10. Maugeri-Sacca M, Bartucci M, De Maria R. DNA damage repair pathways in cancer stem cells. *Mol Cancer Ther* **2012**;11(8):1627-36 doi 10.1158/1535-7163.MCT-11-1040.
11. Ropolo M, Daga A, Griffero F, Foresta M, Casartelli G, Zunino A, *et al.* Comparative analysis of DNA repair in stem and nonstem glioma cell cultures. *Mol Cancer Res* **2009**;7(3):383-92 doi 10.1158/1541-7786.MCR-08-0409.
12. Eyler CE, Rich JN. Survival of the fittest: cancer stem cells in therapeutic resistance and angiogenesis. *J Clin Oncol* **2008**;26(17):2839-45 doi 10.1200/JCO.2007.15.1829.
13. Pilie PG, Gay CM, Byers LA, O'Connor MJ, Yap TA. PARP Inhibitors: Extending Benefit Beyond BRCA-Mutant Cancers. *Clinical cancer research : an official journal of the American Association for Cancer Research* **2019**;25(13):3759-71 doi 10.1158/1078-0432.CCR-18-0968.
14. Robins HI, Zhang P, Gilbert MR, Chakravarti A, de Groot JF, Grimm SA, *et al.* A randomized phase I/II study of ABT-888 in combination with temozolomide in recurrent temozolomide resistant glioblastoma: an NRG oncology RTOG group study. *J Neurooncol* **2016**;126(2):309-16 doi 10.1007/s11060-015-1966-z.
15. Middleton MR, Friedlander P, Hamid O, Daud A, Plummer R, Falotico N, *et al.* Randomized phase II study evaluating veliparib (ABT-888) with temozolomide in patients with metastatic melanoma. *Ann Oncol* **2015**;26(10):2173-9 doi 10.1093/annonc/mdv308.
16. Wang B, Chu D, Feng Y, Shen Y, Aoyagi-Scharber M, Post LE. Discovery and Characterization of (8S,9R)-5-Fluoro-8-(4-fluorophenyl)-9-(1-methyl-1H-1,2,4-triazol-5-yl)-2,7,8,9-tetrahydro-3H-pyrido[4,3,2-de]phthalazin-3-one (BMN 673, Talazoparib), a Novel, Highly Potent, and Orally

- Efficacious Poly(ADP-ribose) Polymerase-1/2 Inhibitor, as an Anticancer Agent. *J Med Chem* **2016**;59(1):335-57 doi 10.1021/acs.jmedchem.5b01498.
17. Murai J, Huang SY, Renaud A, Zhang Y, Ji J, Takeda S, *et al.* Stereospecific PARP trapping by BMN 673 and comparison with olaparib and rucaparib. *Mol Cancer Ther* **2014**;13(2):433-43 doi 10.1158/1535-7163.MCT-13-0803.
 18. Boukerroucha M, Josse C, Segers K, El-Guendi S, Freres P, Jerusalem G, *et al.* BRCA1 germline mutation and glioblastoma development: report of cases. *BMC Cancer* **2015**;15:181 doi 10.1186/s12885-015-1205-1.
 19. Rasmussen RD, Gajjar MK, Tuckova L, Jensen KE, Maya-Mendoza A, Holst CB, *et al.* BRCA1-regulated RRM2 expression protects glioblastoma cells from endogenous replication stress and promotes tumorigenicity. *Nat Commun* **2016**;7:13398 doi 10.1038/ncomms13398.
 20. Saito N, Fu J, Zheng S, Yao J, Wang S, Liu DD, *et al.* A high Notch pathway activation predicts response to gamma secretase inhibitors in proneural subtype of glioma tumor-initiating cells. *Stem cells* **2014**;32(1):301-12 doi 10.1002/stem.1528.
 21. Gyori BM, Venkatachalam G, Thiagarajan PS, Hsu D, Clement MV. OpenComet: an automated tool for comet assay image analysis. *Redox Biol* **2014**;2:457-65 doi 10.1016/j.redox.2013.12.020.
 22. Koul D, Fu J, Shen R, LaFortune TA, Wang S, Tiao N, *et al.* Antitumor activity of NVP-BKM120--a selective pan class I PI3 kinase inhibitor showed differential forms of cell death based on p53 status of glioma cells. *Clin Cancer Res* **2012**;18(1):184-95 doi 10.1158/1078-0432.CCR-11-1558.
 23. Ritchie ME, Phipson B, Wu D, Hu Y, Law CW, Shi W, *et al.* limma powers differential expression analyses for RNA-sequencing and microarray studies. *Nucleic Acids Res* **2015**;43(7):e47 doi 10.1093/nar/gkv007.
 24. Subramanian A, Tamayo P, Mootha VK, Mukherjee S, Ebert BL, Gillette MA, *et al.* Gene set enrichment analysis: a knowledge-based approach for interpreting genome-wide expression profiles. *Proc Natl Acad Sci U S A* **2005**;102(43):15545-50 doi 10.1073/pnas.0506580102.
 25. Szerlip NJ, Pedraza A, Chakravarty D, Azim M, McGuire J, Fang Y, *et al.* Intratumoral heterogeneity of receptor tyrosine kinases EGFR and PDGFRA amplification in glioblastoma defines subpopulations with distinct growth factor response. *Proc Natl Acad Sci U S A* **2012**;109(8):3041-6 doi 10.1073/pnas.1114033109.
 26. Furnari FB, Cloughesy TF, Cavenee WK, Mischel PS. Heterogeneity of epidermal growth factor receptor signalling networks in glioblastoma. *Nat Rev Cancer* **2015**;15(5):302-10 doi 10.1038/nrc3918.
 27. Francis JM, Zhang CZ, Maire CL, Jung J, Manzo VE, Adalsteinsson VA, *et al.* EGFR variant heterogeneity in glioblastoma resolved through single-nucleus sequencing. *Cancer Discov* **2014**;4(8):956-71 doi 10.1158/2159-8290.CD-13-0879.
 28. Ran FA, Hsu PD, Lin CY, Gootenberg JS, Konermann S, Trevino AE, *et al.* Double nicking by RNA-guided CRISPR Cas9 for enhanced genome editing specificity. *Cell* **2013**;154(6):1380-9 doi 10.1016/j.cell.2013.08.021.
 29. Mali P, Yang L, Esvelt KM, Aach J, Guell M, DiCarlo JE, *et al.* RNA-guided human genome engineering via Cas9. *Science* **2013**;339(6121):823-6 doi 10.1126/science.1232033.
 30. Nitta M, Kozono D, Kennedy R, Stommel J, Ng K, Zinn PO, *et al.* Targeting EGFR induced oxidative stress by PARP1 inhibition in glioblastoma therapy. *PLoS One* **2010**;5(5):e10767 doi 10.1371/journal.pone.0010767.
 31. Murai J, Huang SY, Das BB, Renaud A, Zhang Y, Doroshow JH, *et al.* Trapping of PARP1 and PARP2 by Clinical PARP Inhibitors. *Cancer Res* **2012**;72(21):5588-99 doi 10.1158/0008-5472.CAN-12-2753.

32. Mellinghoff IK, Wang MY, Vivanco I, Haas-Kogan DA, Zhu S, Dia EQ, *et al.* Molecular determinants of the response of glioblastomas to EGFR kinase inhibitors. *N Engl J Med* **2005**;353(19):2012-24 doi 10.1056/NEJMoa051918.
33. Verhaak RG, Hoadley KA, Purdom E, Wang V, Qi Y, Wilkerson MD, *et al.* Integrated genomic analysis identifies clinically relevant subtypes of glioblastoma characterized by abnormalities in PDGFRA, IDH1, EGFR, and NF1. *Cancer cell* **2010**;17(1):98-110 doi 10.1016/j.ccr.2009.12.020.
34. Mendes-Pereira AM, Martin SA, Brough R, McCarthy A, Taylor JR, Kim JS, *et al.* Synthetic lethal targeting of PTEN mutant cells with PARP inhibitors. *EMBO Mol Med* **2009**;1(6-7):315-22 doi 10.1002/emmm.200900041.
35. Lehtio L, Jemth AS, Collins R, Loseva O, Johansson A, Markova N, *et al.* Structural basis for inhibitor specificity in human poly(ADP-ribose) polymerase-3. *J Med Chem* **2009**;52(9):3108-11 doi 10.1021/jm900052j.
36. Sulkowski PL, Corso CD, Robinson ND, Scanlon SE, Purshouse KR, Bai H, *et al.* 2-Hydroxyglutarate produced by neomorphic IDH mutations suppresses homologous recombination and induces PARP inhibitor sensitivity. *Sci Transl Med* **2017**;9(375) doi 10.1126/scitranslmed.aal2463.
37. Ning JF, Stanciu M, Humphrey MR, Gorham J, Wakimoto H, Nishihara R, *et al.* Myc targeted CDK18 promotes ATR and homologous recombination to mediate PARP inhibitor resistance in glioblastoma. *Nat Commun* **2019**;10(1):2910 doi 10.1038/s41467-019-10993-5.
38. Lu Y, Kwintkiewicz J, Liu Y, Tech K, Frady LN, Su YT, *et al.* Chemosensitivity of IDH1-Mutated Gliomas Due to an Impairment in PARP1-Mediated DNA Repair. *Cancer Res* **2017**;77(7):1709-18 doi 10.1158/0008-5472.CAN-16-2773.
39. Lu Y, Liu Y, Pang Y, Pacak K, Yang C. Double-barreled gun: Combination of PARP inhibitor with conventional chemotherapy. *Pharmacol Ther* **2018**;188:168-75 doi 10.1016/j.pharmthera.2018.03.006.
40. Tateishi K, Higuchi F, Miller JJ, Koerner MVA, Lelic N, Shankar GM, *et al.* The Alkylating Chemotherapeutic Temozolomide Induces Metabolic Stress in IDH1-Mutant Cancers and Potentiates NAD(+) Depletion-Mediated Cytotoxicity. *Cancer Res* **2017**;77(15):4102-15 doi 10.1158/0008-5472.CAN-16-2263.
41. Johnson B, Chandra J. Abstract 511: EGFR-initated NADPH oxidase activity regulates Fyn expression in glioblastoma multiforme. *Cancer Research* **2014**;74(19 Supplement):511- doi 10.1158/1538-7445.am2014-511.
42. Ryu JW, Choe SS, Ryu SH, Park EY, Lee BW, Kim TK, *et al.* Paradoxical induction of growth arrest and apoptosis by EGF via the up-regulation of PTEN by activating Redox factor-1/Egr-1 in human lung cancer cells. *Oncotarget* **2017**;8(3):4181-95 doi 10.18632/oncotarget.13809.
43. Chen X, Abair TD, Ibanez MR, Su Y, Frey MR, Dise RS, *et al.* Integrin alpha1beta1 controls reactive oxygen species synthesis by negatively regulating epidermal growth factor receptor-mediated Rac activation. *Mol Cell Biol* **2007**;27(9):3313-26 doi 10.1128/MCB.01476-06.
44. Paulsen CE, Truong TH, Garcia FJ, Homann A, Gupta V, Leonard SE, *et al.* Peroxide-dependent sulfenylation of the EGFR catalytic site enhances kinase activity. *Nat Chem Biol* **2011**;8(1):57-64 doi 10.1038/nchembio.736.
45. Truong TH, Ung PM, Palde PB, Paulsen CE, Schlessinger A, Carroll KS. Molecular Basis for Redox Activation of Epidermal Growth Factor Receptor Kinase. *Cell Chem Biol* **2016**;23(7):837-48 doi 10.1016/j.chembiol.2016.05.017.
46. Leung EL, Fan XX, Wong MP, Jiang ZH, Liu ZQ, Yao XJ, *et al.* Targeting Tyrosine Kinase Inhibitor-Resistant Non-Small Cell Lung Cancer by Inducing Epidermal Growth Factor Receptor Degradation via Methionine 790 Oxidation. *Antioxid Redox Signal* **2016**;24(5):263-79 doi 10.1089/ars.2015.6420.

47. Kizilbash SH, Gupta SK, Chang K, Kawashima R, Parrish KE, Carlson BL, *et al.* Restricted Delivery of Talazoparib Across the Blood-Brain Barrier Limits the Sensitizing Effects of PARP Inhibition on Temozolomide Therapy in Glioblastoma. *Mol Cancer Ther* **2017**;16(12):2735-46 doi 10.1158/1535-7163.MCT-17-0365.
48. Gupta SK, Mladek AC, Carlson BL, Boakye-Agyeman F, Bakken KK, Kizilbash SH, *et al.* Discordant in vitro and in vivo chemopotentiating effects of the PARP inhibitor veliparib in temozolomide-sensitive versus -resistant glioblastoma multiforme xenografts. *Clinical cancer research : an official journal of the American Association for Cancer Research* **2014**;20(14):3730-41 doi 10.1158/1078-0432.CCR-13-3446.
49. Parrish KE, Cen L, Murray J, Calligaris D, Kizilbash S, Mittapalli RK, *et al.* Efficacy of PARP Inhibitor Rucaparib in Orthotopic Glioblastoma Xenografts Is Limited by Ineffective Drug Penetration into the Central Nervous System. *Mol Cancer Ther* **2015**;14(12):2735-43 doi 10.1158/1535-7163.MCT-15-0553.

Figure Legends

Fig. 1. Talazoparib effectively inhibited the proliferation of EGFR-amplified GSCs. A test set of GSCs (A-B) and a validation set of GSCs (C-D) were treated with 0.32 nM to 1000 nM talazoparib for 5 days; cell viability was assessed using a CellTiter-Blue assay. Waterfall diagrams of IC₅₀ and the genetic status of GSCs are shown. (E-H) Dot blots showing the correlation between EGFR, p53, PTEN, and CDKN2A status and in vitro drug sensitivity, as shown by the IC₅₀ of individual GSCs. Lines indicate medians with interquartile ranges. (I) EGFR copy number variation (CNV) determined by OncoScan® FFPE Assay. CNV=2 was set as a threshold for amplification. (J) Representative FISH pictures to show EGFR amplification. Green: *EGFR* signals; blue: 4',6-diamidino-2-phenylindole (DAPI). Scale bar, 10 μm. (K) Quantification for FISH results, at least 50 cells were analyzed for each cell line. (L) Western blot for EGFR expression and signaling in test set of GSCs.

Fig.2. Depletion of EGFR renders resistance to talazoparib. (A-C) EGFR was knocked out by CRISPR in GSC262 cells, and depletion of EGFR expression and signaling was confirmed by Western blot analysis (A), cell viability in response to 5 days of talazoparib treatment was evaluated using the CellTiter-Blue assay (B), and the IC₅₀ was calculated using GraphPad software (C). (D-I) EGFR-amplified GSC274 and GSC11 were transfected with shRNAs targeting EGFR (EGFR-sh1 and EGFR-sh2) or scramble (SCR), and EGFR expression and signaling was confirmed by Western blot (D and G). Cell viability in response to 5 days of talazoparib treatment was evaluated using the CellTiter-Blue assay (E and H), and IC₅₀ of talazoparib was calculated using GraphPad software (F and I). (G-I) Wild type EGFR (EGFR-wt) and EGFR kinase-inactive mutant (EGFR-KI) were overexpressed in GSC272 cells, and EGFR expression was detected by Western blot analysis (G). Cell viability in response to 5 days of talazoparib treatment was evaluated using the CellTiter-Blue assay (H), and the IC₅₀ was calculated using GraphPad (I). Bar plots represent mean± SD from 3 independent experiments.

Fig. 3. Elevated baseline ROS in EGFR-amplified GSCs and related to talazoparib sensitivity. (A) ROS was measured in GSCs by flow cytometry analysis using the general oxidative stress indicator CM-H2DCFDA and a dot plot showing a correlation between EGFR status and ROS level. (B) ROS was measured in GSC262-vector and GSC262 EGFR knock-out (EGFR-KO) cells (C) Dose-response curves of EGFR-amplified cells and non-amplified cells to talazoparib with or without ROS-specific inhibitor MnTBAP. (D) Dose-response curves of GSC262 vector and EGFR CRISPR knock-out cells were to talazoparib with or without ROS-specific inhibitor MnTBAP. (E) GSCs were treated with 100nM talazoparib for 48 hours, 8-OHdG was measured by OxiSelect™ Oxidative DNA Damage ELISA kit. Results for all bar plots represent the mean± SD from three independent experiments.

Fig. 4. Increased DNA damage in EGFR-amplified GSC. (A) Upregulation of DNA damage repair signatures in EGFR-amplified GSC cell lines, as determined by gene set enrichment analysis. The X-axis represents genes, ordered by expression changes between amplified and non-amplified. The Y-axis represents the cumulative enrichment score. (B) EGFR-amplified and

non-amplified GSCs were treated with talazoparib at 100 nM for 72 hours and DNA damage was evaluated by γ H2AX (red) and 53BP1 (green) staining. (C) Comet assay in GSC262-vector and GSC262 EGFR CRISPR knock-out cells treated with talazoparib for indicated time. DNA damage quantified via the percentage DNA in tails. Each data point represents at least 50 cells counted. GSC262 vector and GSC262 EGFR CRISPR knock-out cells (D), and GSC272 vector and overexpressing EGFR (E) were treated with talazoparib 100 nM for 72 hours, and then washed out talazoparib for indicated time, DNA repair was evaluated by γ H2AX (red) and 53BP1 (green) staining. Scale bar, 20 μ m for B, D and E, 100 μ m for C. For D, F and G, each data point represent 3 fields with over 30 cells/field. Symbol * indicates $P < 0.05$.

Fig. 5. Talazoparib traps the PARP-DNA complex in EGFR-amplified GSCs. (A-C) EGFR amplified GSC262 (A), GSC274 (B), and non-amplified GSC272 (C) cells were treated with 100 nM talazoparib for 3 days and 5 days. Cytoplasmic, nuclear soluble, and chromatin-bound fractions were analyzed for PARP expression by Western blot. Actin, Lamin B, and Histone 3 were used as markers for cytoplasm, nuclear and chromatin-bound, respectively. (D) GSC262 vector cells and EGFR CRISPR knock-out cells (KO) were treated with 100 nM talazoparib for 5 days. Cytoplasmic, nuclear soluble, and chromatin-bound fractions were analyzed for PARP by Western blot analysis. (E) GSC272 expressing empty vector (GSC272 vector) and GSC272 overexpressing EGFR (GSC272-EGFR) cells were treated with 100 nM talazoparib for 5 days. Cytoplasmic, nuclear soluble, and chromatin-bound fractions were analyzed for PARP by Western blot analysis. The expression of PARP was quantified by Image-J, and percentage of PARP trapped to chromatin was calculated as chromatin-bound PARP/ (chromatin-bound PARP+ soluble nuclear PARP) % and was shown at the bottom.

Fig.6. Comparing in vivo efficacy of talazoparib in EGFR-amplified and non-amplified models. (A-D) EGFR-amplified cells GSC262 (A, n=5 per group) and GSC11 (B, n=6 per group), EGFR non-amplified GSC272 (C, n=4 per group) and GSC23 (D, n=3 per group) were implanted to nude mice to establish subcutaneous models. Mice were administrated with talazoparib (0.33 mg/kg) or vehicle for 6 weeks for GSC262 and GSC23. GSC11 and GSC272 were treated for only 5 weeks as the tumor burden exceeded the limit. Representative bioluminescent imaging of tumor was shown (Top panels). Tumor growth was evaluated by normalizing to bioluminescence at treatment start (Bottom panels). (E) Representative images of the immunohistochemistry analyses of xenograft tumors with anti- γ H2AX and cleaved caspase-3. (F) Mice bearing EGFR-amplified GSC262 intracranial tumors (G-I) or non-amplified GSC272 (J-L) were administrated with talazoparib (0.33 mg/kg) or vehicle. Representative bioluminescent imaging of tumor was shown (G and J). Tumor growth was evaluated by normalizing to bioluminescence at treatment start (H and K). Survival curves were compared using Kaplan-Meier survival plots (I and L). Scale bar, 50 μ m for E and F. Symbol * indicates $P < 0.05$.

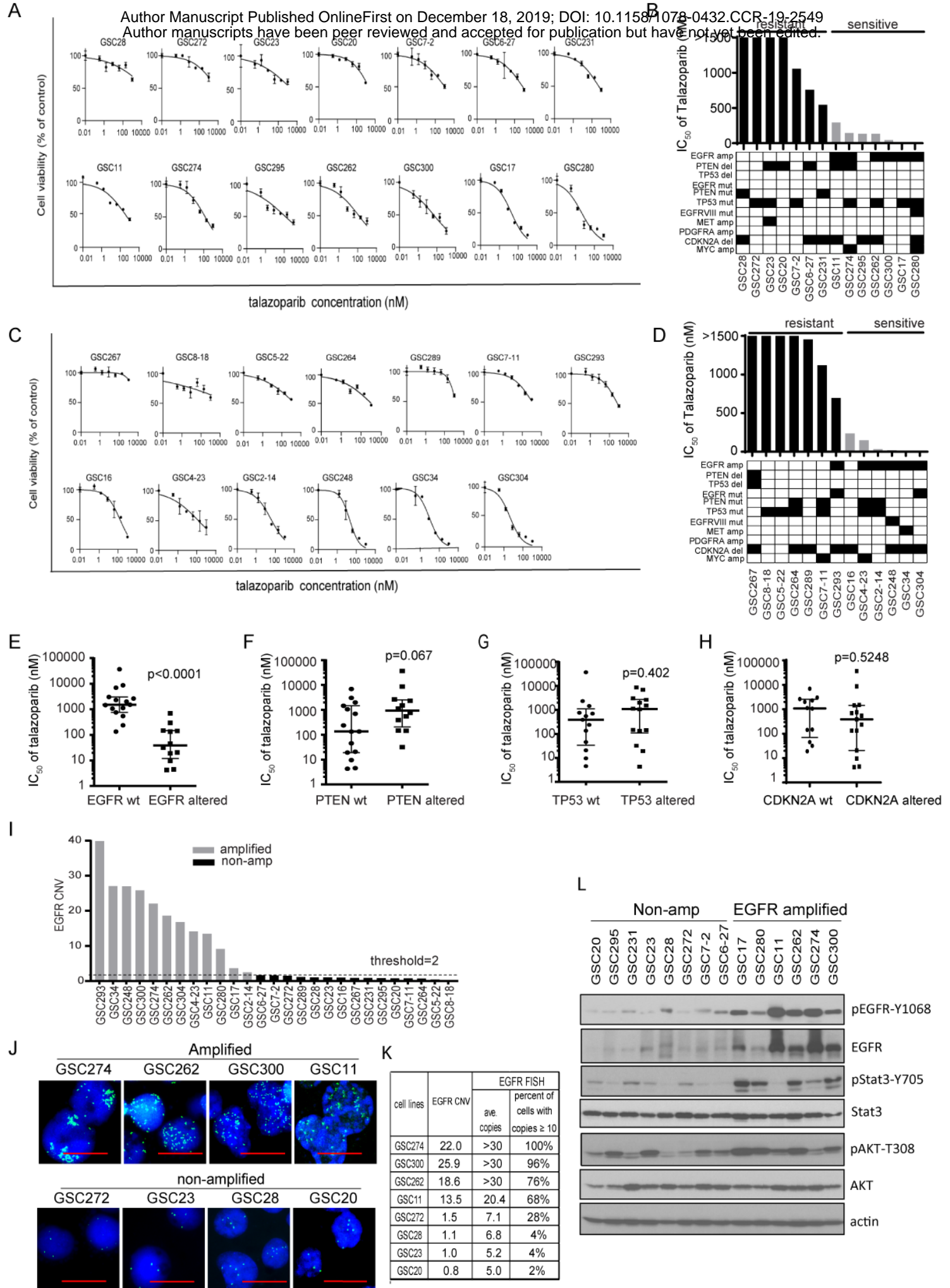
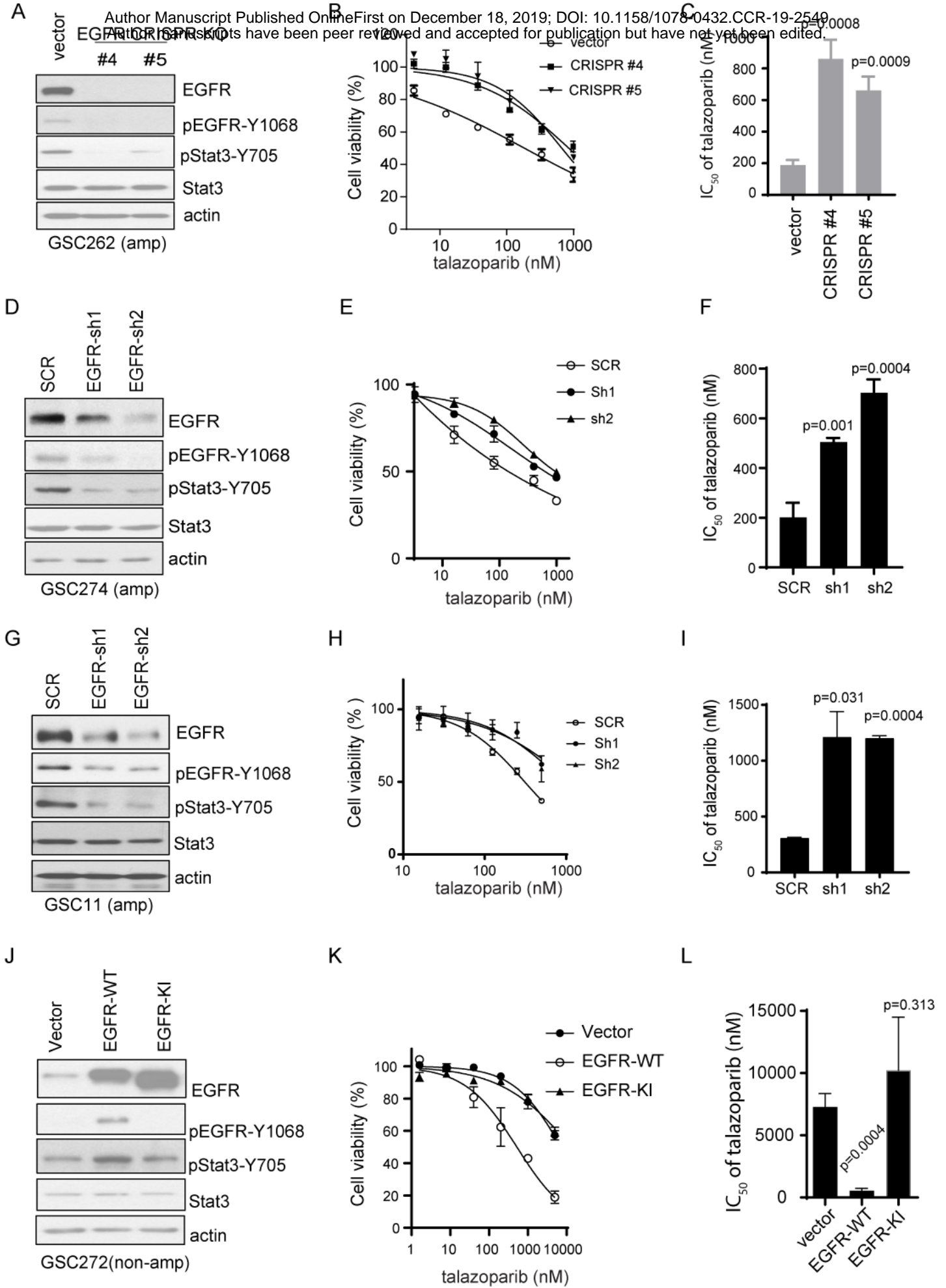
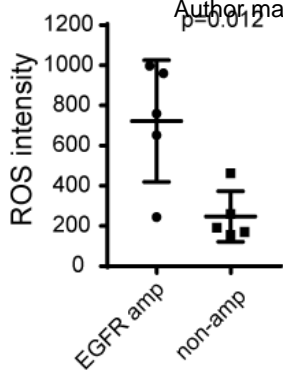


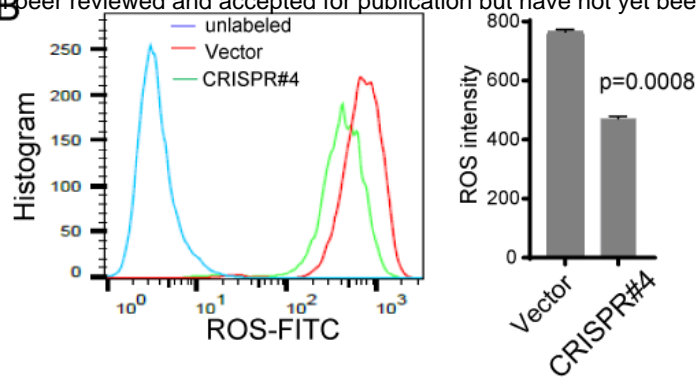
Figure 1



A

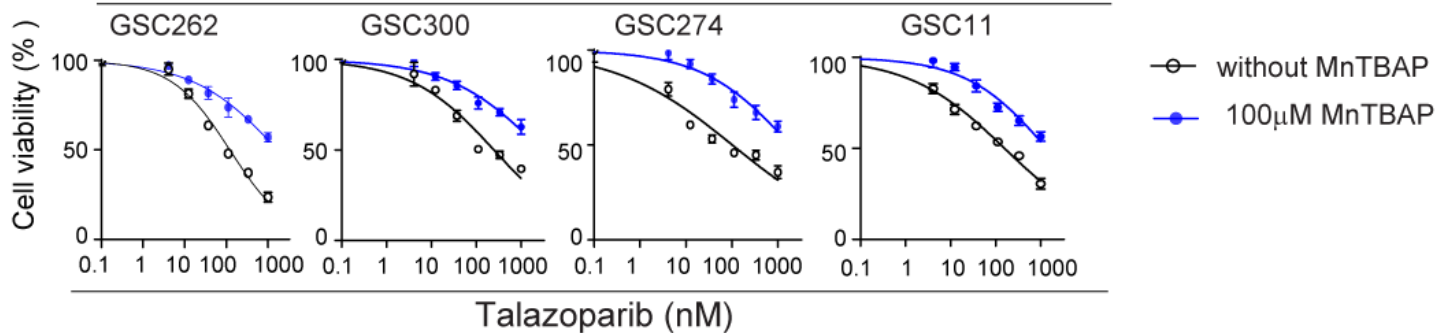


B

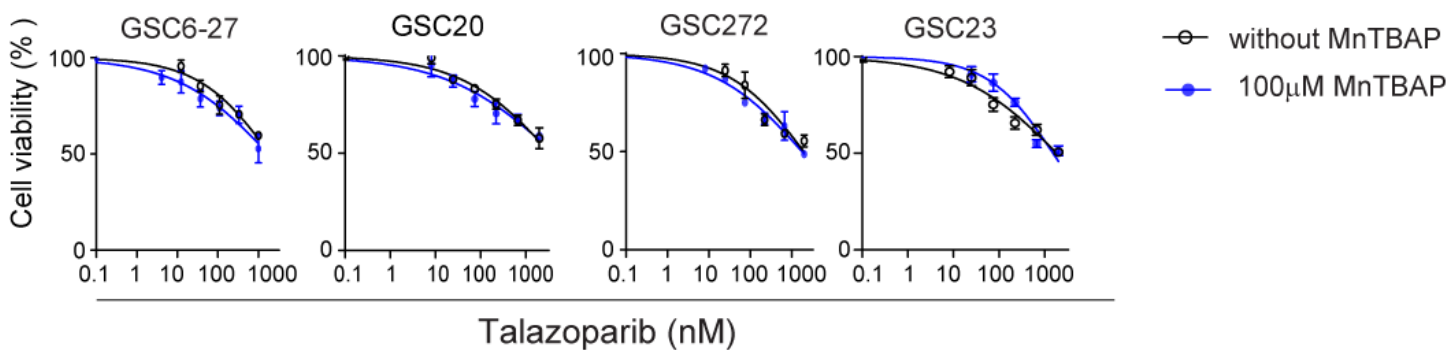


C

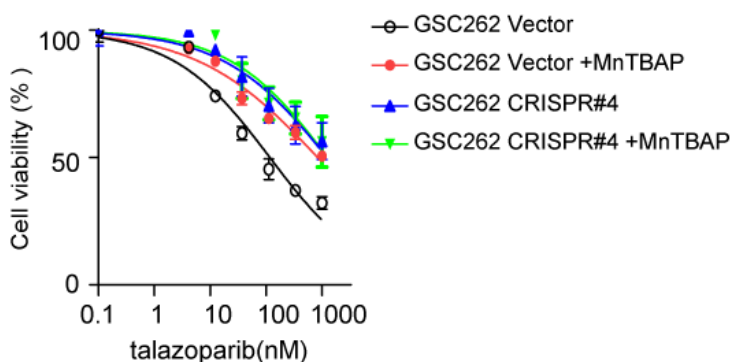
EGFR-amplified



EGFR-non-amplified



D



E

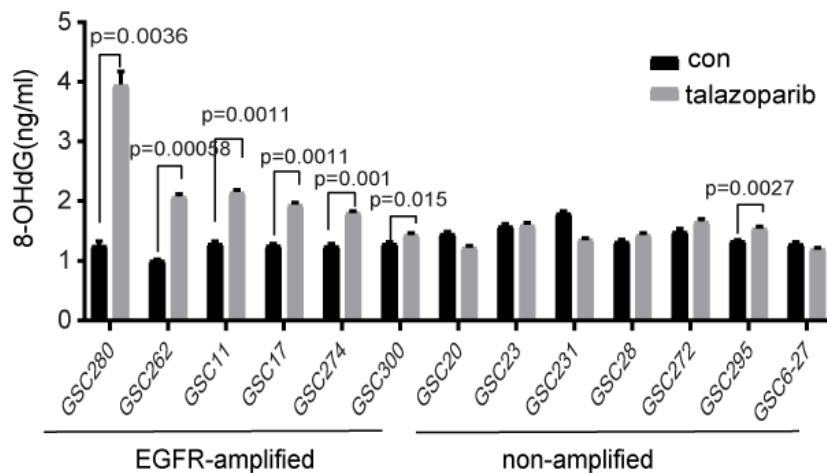
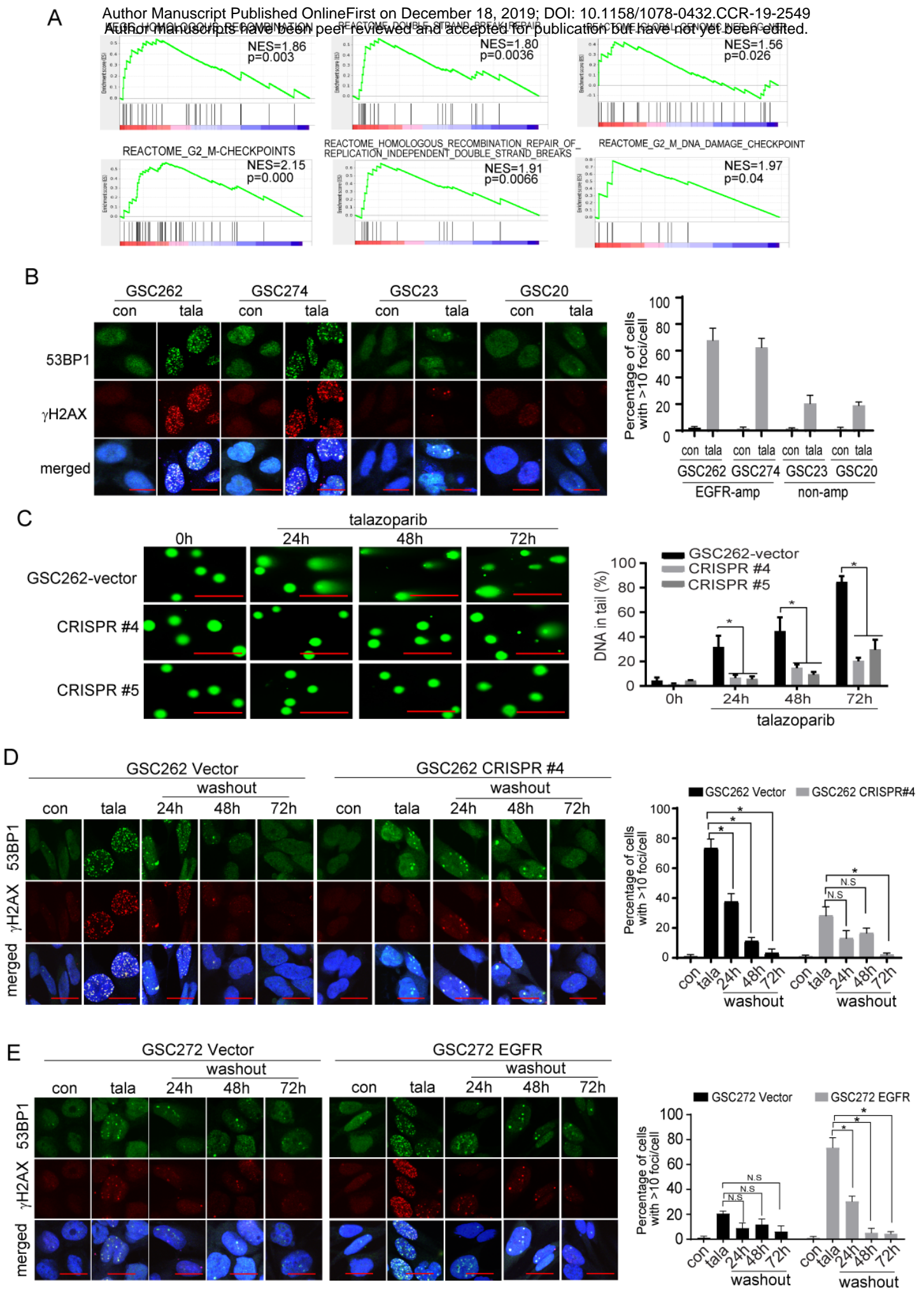


Figure 3



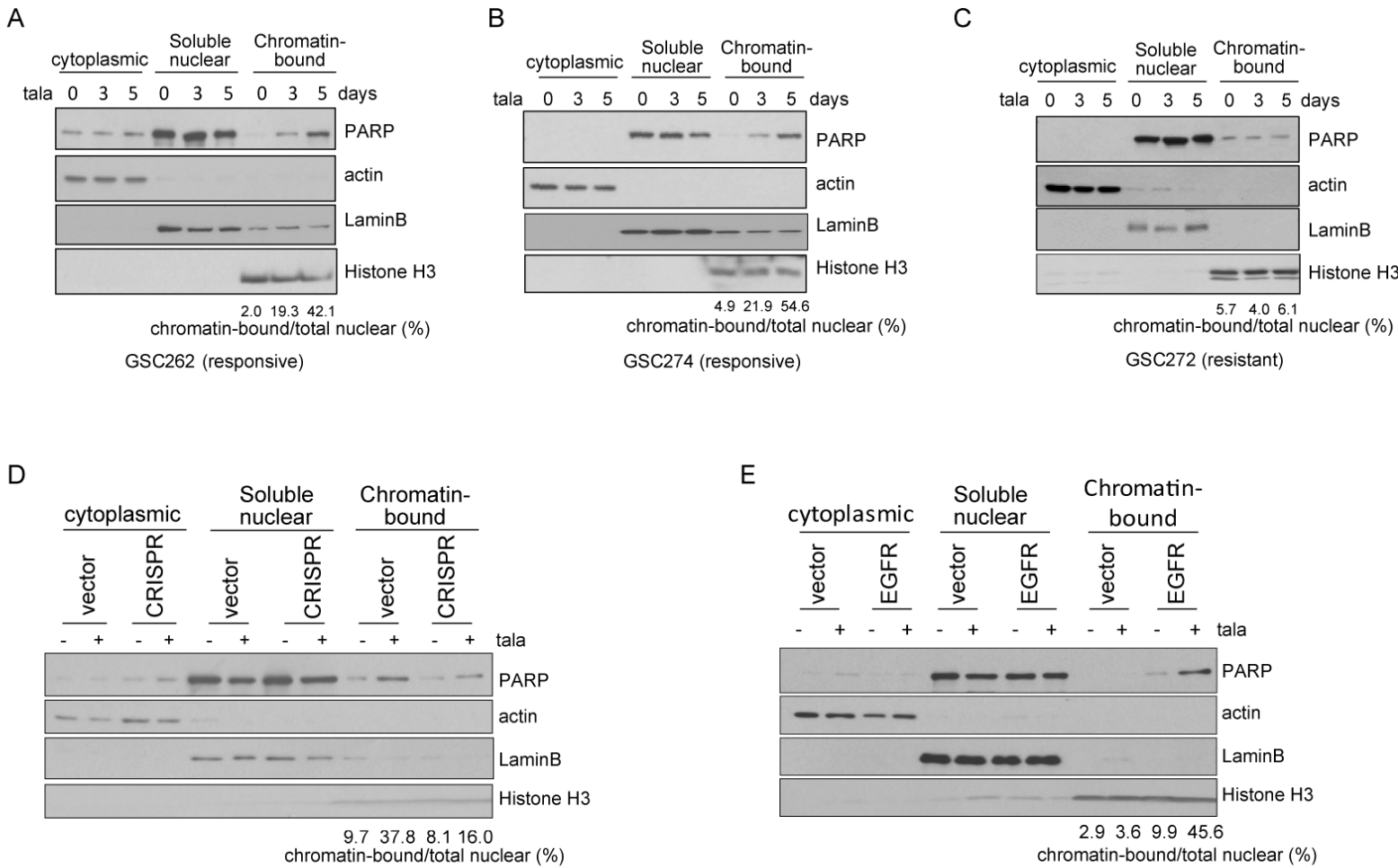
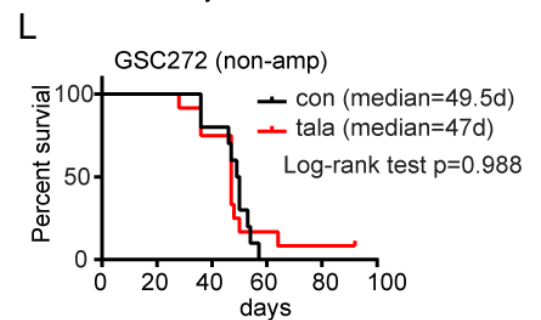
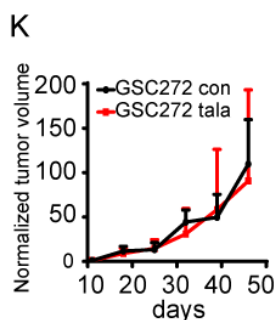
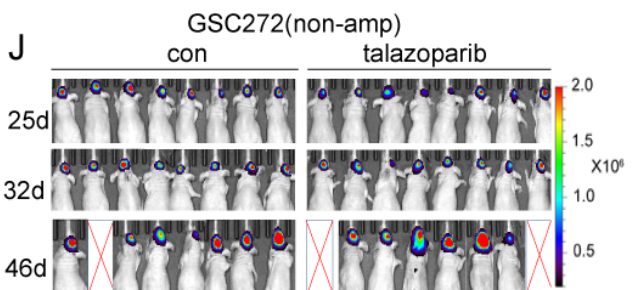
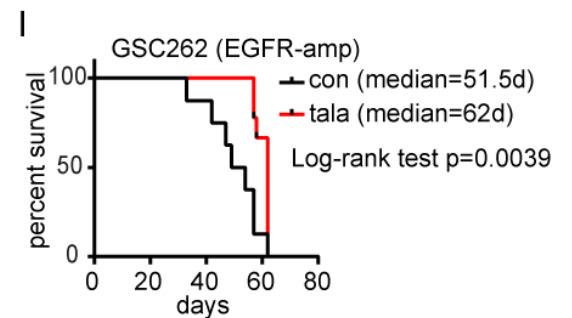
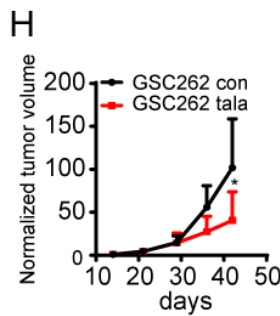
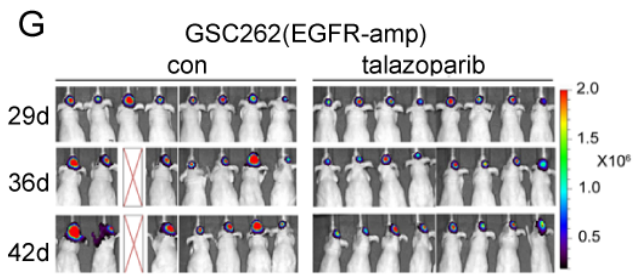
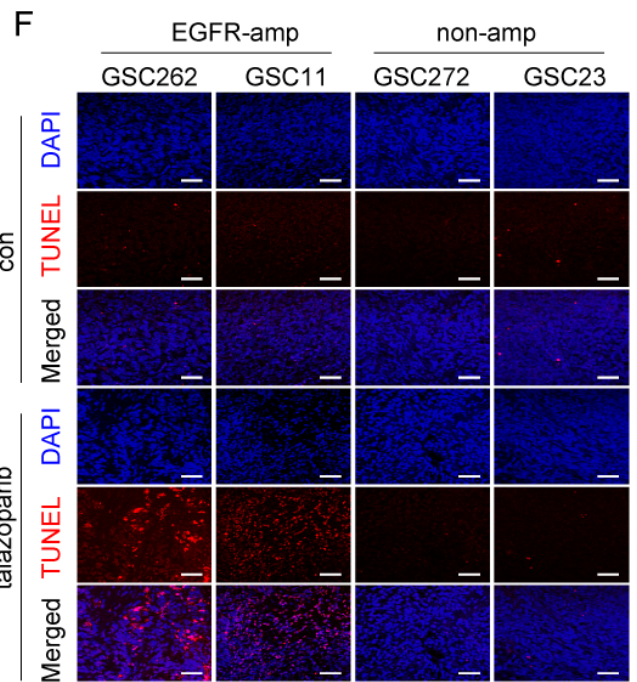
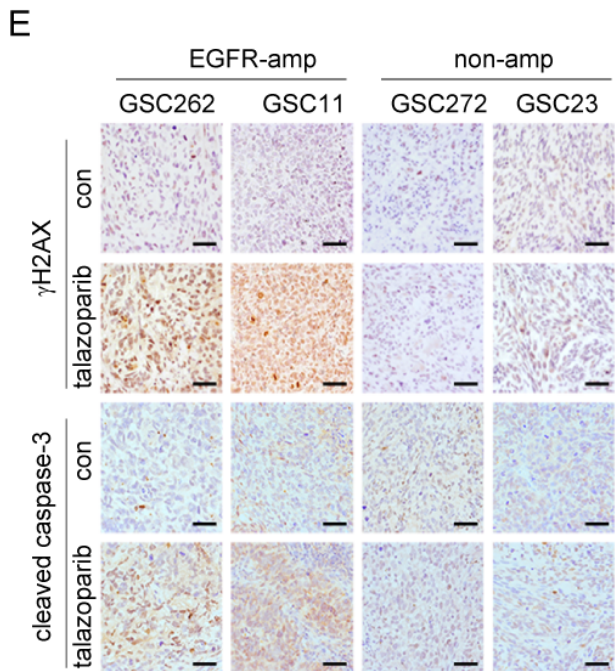
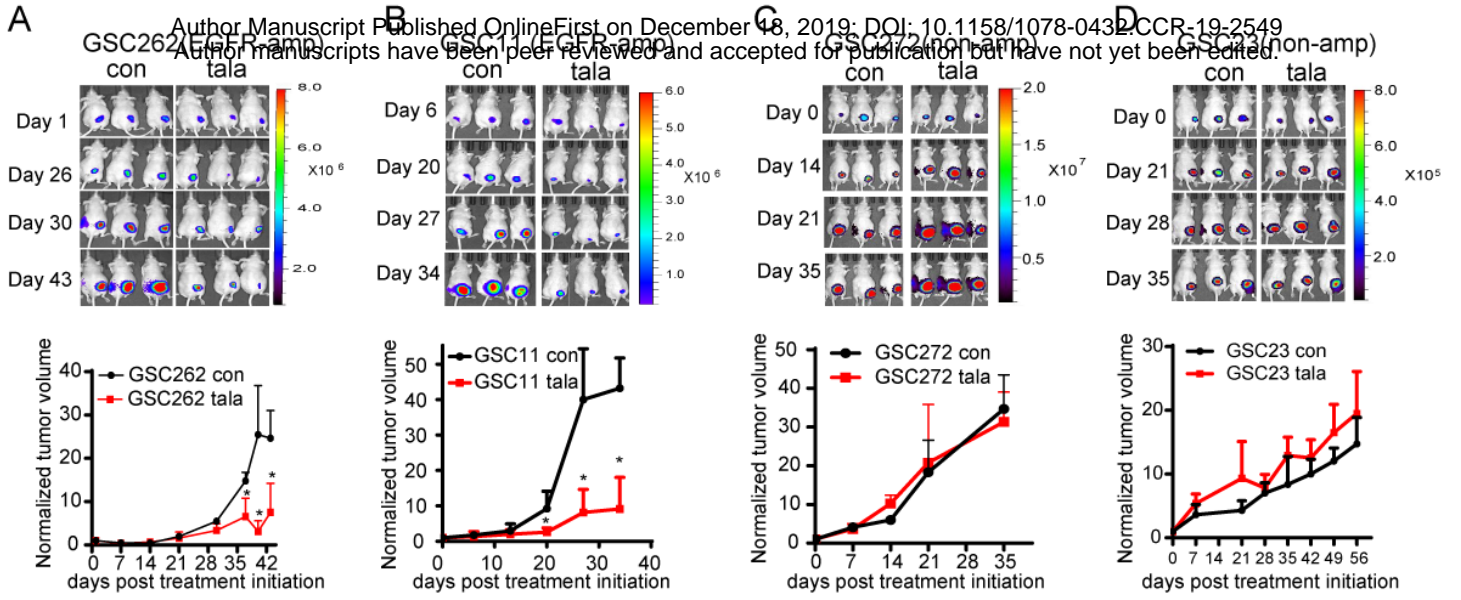


Fig 5



Clinical Cancer Research

EGFR amplification induces increased DNA damage response and renders selective sensitivity to Talazoparib (PARP inhibitor) in glioblastoma

Shaofang Wu, Feng Gao, Siyuan Zheng, et al.

Clin Cancer Res Published OnlineFirst December 18, 2019.

Updated version	Access the most recent version of this article at: doi: 10.1158/1078-0432.CCR-19-2549
Supplementary Material	Access the most recent supplemental material at: http://clincancerres.aacrjournals.org/content/suppl/2019/12/18/1078-0432.CCR-19-2549.DC1
Author Manuscript	Author manuscripts have been peer reviewed and accepted for publication but have not yet been edited.

E-mail alerts	Sign up to receive free email-alerts related to this article or journal.
Reprints and Subscriptions	To order reprints of this article or to subscribe to the journal, contact the AACR Publications Department at pubs@aacr.org .
Permissions	To request permission to re-use all or part of this article, use this link http://clincancerres.aacrjournals.org/content/early/2019/12/18/1078-0432.CCR-19-2549 . Click on "Request Permissions" which will take you to the Copyright Clearance Center's (CCC) Rightslink site.